Journal of Nuclear Materials 392 (2009) 105–113

Contents lists available at ScienceDirect

Journal of Nuclear Materials

journal homepage: www.elsevier.com/locate/jnucmat

Deformation twinning and twinning related fracture in coarse-grained α-uranium

R.D. Field *, R.J. McCabe, D.J. Alexander, D.F. Teter

Materials Science and Technology – MST-6, M.S. G770, Los Alamos National Laboratory, Los Alamos, NM 87545, USA

ARTICLE INFO

Article history:
Received 23 June 2008
Accepted 24 March 2009

ABSTRACT

An investigation of deformation twinning in coarse-grained α-uranium was conducted within the heat-affected zone of weld specimens tested in tension. Twins and twin interactions were studied both at fracture surfaces and sub-surface, using transmission electron microscopy (TEM) and electron backscatter diffraction (EBSD). The fracture surface plane was identified using TEM of foils cut from the fracture surface using a focused ion beam. Intersecting twins found in these foils were also analyzed. EBSD was also used to analyze twins and twin interactions at and below the fracture surface. Fracture parallel to {172} twin planes and {172} twin crossings were observed, in agreement with previous optical/Laue diffraction studies. Previously unobserved crossings of {172} twins by {112} twins were also frequently observed. These twin interactions are interpreted in terms of previously established crystallographic criteria for twin crossings.

1. Introduction

Deformation and fracture of α-uranium (α-U) is an interesting topic because of the abundance of deformation systems available in the orthorhombic structure, including several different twinning systems. Uranium exhibits compound, Type I, and Type II twins, the only metal known to do so, and interactions between these twins are often complex. Several seminal works regarding deformation twinning are based on research of α-U [1–3].

The earliest work to identify twinning modes in α-U was from Cahn [1]. Several twinning systems were identified, including the compound {130}/⟨310⟩ system (K_1 and η_1, respectively), Type I {112}/⟨372⟩, and Type II {172}/⟨312⟩, where ⟨372⟩ and {172} are approximations of irrational indices. A tentative identification of a {121} twin was also made. Frank [3] analyzed the twinning modes found by Cahn in terms of known twinning modes in hcp crystals, since α-U can be considered as a distorted hexagonal structure.

Lloyd and Chiswik [4] confirmed the {1 3 0} and {1 7 2} twinning systems. In addition, they observed a {1 7 6}/[5 1 2] Type II twinning system (again, the K_1 indices are approximations of irrational values). Daniel et al. [5] also confirmed the presence of {1 3 0} and {1 7 6} twins, although they approximated the K_1 plane of the latter as {1 9 7}, after Crocker. Crocker [2] performed a complete theoretical analysis of twins in the structure, including the influence of shuffles. This work represented a major advance in the understanding of shuffles in twinning mechanisms. Of particular interest is his explanation of the increased mobility of {1 3 0} twins, which involve simple shuffles, compared to other systems that have smaller shears but require more complex shuffles to restore the crystal structure.

Cahn [1] identified fracture planes associated with {172} twins in his specimens, which he likened to 'parting' mechanisms in minerals. This observation was later confirmed by others, with additional evidence for parting along {121} and possibly {112} twins [6,7]. This phenomenon is more prevalent in single crystals and large grained polycrystals and at low temperatures, primarily due to the increased twin activity under these conditions [8]. It is generally agreed that twin boundaries represent high energy sites for crack propagation, particularly {172} twins, which are expected to have a particularly high degree of disorder due to shuffle requirements at the twin/matrix interface [6,8,9], as noted by Crocker [2]. Their role in nucleation is less certain, with some maintaining that cracks are nucleated at apexes of twins by accommodation strains [8] and others proposing slip dislocation interactions with twins and low angle boundaries as principal nucleation mechanisms [6,7].

Recent advances in experimental techniques for studying deformation structures warrant a reexamination of twinning and fracture in α-U. Two specific techniques were applied to this problem. Electron backscattered diffraction (EBSD), sometimes referred to as orientation imaging microscopy (OIM), has been recently used to investigate deformation twins in α-U [10–13]. A significant number of {130} deformation twins have been observed for fine-grained α-U having undergone quasi-static loading [13] and shock wave loading [12], with {172}, and {112} twins also being observed in smaller numbers. The second is a very recent technique in which focused ion beam (FIB) combined with transmission electron microscopy (TEM) is used to determine the crystallographic orientation of a flat (i.e., cleavage or

* Corresponding author. Tel.: +1 505 663 5807; fax: +1 505 667 5268.
E-mail addresses: rdfield@lanl.gov, rfields101@comcast.net (R.D. Field).

0022-3115/$ - see front matter © 2009 Elsevier B.V. All rights reserved.
doi:10.1016/j.jnucmat.2009.03.054

quasi-cleavage) fracture surface [14]. Application of these techniques has yielded new insight into twinning mechanisms and fracture in α-U.

2. Experimental procedure

The starting material was commercial grade, rolled and annealed plate. Results from chemical analysis are shown in Table 1. This material is typically hot rolled at 600 °C (high-α) in several passes with 90° rotation between passes to a total reduction of approximately 50% to break up the cast structure. It is then clock rolled at 300 °C to a further reduction of approximately 50%, with one intermediate anneal at 600 °C/15 min., followed by a final 550 °C/1 h anneal to yield an approximately 20 μm equiaxed α grain structure. Electron-beam (EB) welds were made using weld parameters that were designed to produce a sound weld.

Base metal material approximately 3.5 mm thick was cut into two strips nominally 50 mm wide. A central groove 19 mm wide was machined along both surfaces of the strip to leave a web that was 0.97 mm thick. The strip was cleaned, and an EB weld was made along the middle of the reduced-thickness web. Tensile samples with a shoulder 25.4 mm wide and a central gage section 12.7 mm wide by 12.7 mm long were oriented transverse to the weld and sectioned by electro-discharge machining. The gage section width was slightly oversized, and 0.13 mm was removed from each side by final machining.

The tensile samples were tested with self-tightening wedge grips that grasped the sample shoulders. Testing was performed at −54 °C; the load train and samples were enclosed in a cooling chamber with a fan that circulated vapor from liquid nitrogen. Thermocouples were located on the grips and on the sample gage section to measure the temperature. Samples were tested with a servohydraulic testing machine at a constant actuator velocity of 0.019 mm/s or 19 mm/s, intended to result in nominal strain rates of 0.001 or 1 s^{-1}, respectively. The low strain rate specimen (interrupted prior to final fracture) was used in the EBSD study, while the fracture surface from the high strain rate test was subjected to TEM analysis. An extensometer with an initial gage length of 12.7 mm and 25% strain capacity was used, so that the extensometer could straddle the weld metal and the heat-affected zone (HAZ).

Specimens were prepared for optical metallography using techniques developed by Kelly et al. [15] and for EBSD using a two-step electropolish process detailed elsewhere [11]. EBSD analysis was also performed on welded specimens prior to tensile testing. Automated EBSD scans were performed at 25 kV in an FEI XL30 ESEM equipped with an EDAX/TSL data acquisition system. Regions were orientation mapped with a step size of 1 μm in a hexagonal grid. The orientation data were analyzed using EDAX/TSL OIM™ Analysis software. Twin boundaries were classified with the OIM software using a misorientation of 180° ± 5° about either K_1 or η_1 depending on whether the twin was Type I or Type II, with either working for the {1 3 0} compound twin.

Specimens for transmission electron microscopy were prepared using an FEI DB235 focused ion instrument. Two specimens were taken from a flat fracture surface at a projected angle of 90° from each other and line direction analysis was performed on the fracture surface/foil interfaces using standard techniques. The cross-product of the two line directions then yielded the fracture plane. Details of this procedure are described elsewhere [14].

Table 1
Chemical analysis data for U plate (all wt. ppm except for U, which is in wt%).

U	Fe	Ni	Cu	Mn	Ti	Zr	C
99.975	61	12	5	7	7	5	65

3. Results and discussion

3.1. Initial weld structure

Fig. 1 shows an optical micrograph and corresponding EBSD inverse pole figure (IPF) map of the initial, unstrained, weld microstructure. The images show the fine-grained parent material as well as the weld and heat-affected zone (HAZ). The initial microstructure within the weld and HAZ consists of millimeter-sized grains with generally only a small number of grains (1–3) spanning the entire thickness of the sample. The large grains are composed of a structure of misoriented (2–15°) sub-grains and {1 3 0} twins. The {1 3 0} twins are believed to be mechanical twins resulting from intergranular stresses that occur during cooling. Similar twins are regularly observed in cast uranium. These twins are active during subsequent deformation, particularly for grains oriented near [1 0 0] in tension. However, {1 7 2} and {1 1 2} twins also play a prominent role in subsequent deformation, and fracture in particular; these twins are the focus of this work.

3.2. Mechanical testing

Fig. 2 shows a tensile bar following an interrupted test at −54 °C and a nominal strain rate of 0.001 s^{-1}. The test was stopped by a sudden drop in load, but the sample did not fail completely. As Fig. 2 shows, several large cracks formed, but did not link up. Cracks occurred in the weld metal, and also in the HAZ (demarcated with dashed lines on the figure) on both sides of the weld metal, suggesting that all of these zones had similar fracture characteristics.

The samples showed a very low failure strain of only about 1.5%. However, this is not the actual fracture strain. Because these are composite tensile specimens, with base metal, weld metal, and heat-affected zone material all included in the gage section, the measured strains are overall strains, not local strains. The base metal is stronger than the weld metal or HAZ, and so resists deformation. Thus, the actual strains are concentrated in the weld metal and HAZ. These microstructures are very inhomogeneous, so the strain is also inhomogeneously distributed in the weld metal and HAZ. Thus, the actual fracture strain is greater than the overall strains as measured by the extensometer, although it is not clear how much greater.

The gage section of the specimen was cut perpendicular to the weld, bisecting the long straight crack shown in the expanded view. The two sections were mounted in epoxy and prepared for metallographic and EBSD analysis, with the section below the cut mounted for cross-sectional analysis and the section above the cut mounted for plan view analysis.

3.3. Determination of fracture surface and surface twin using FIB/TEM

The fracture surface of a specimen tested to failure is shown in the scanning electron micrograph (SEM) of Fig. 3. Fracture occurred within the HAZ, which contains large (millimeter sized) grains. The fracture surface displays several flat regions, decorated by parallel striations. One of these regions was chosen for the FIB/TEM investigation and two foils were removed in the FIB, perpendicular to each other (Fig. 4).

Low magnification TEM images of the two foils used in the analysis are shown in Fig. 5. Most of the fracture surface interface has been removed from foil #1 during the FIB operation. However, a sufficient amount remains to perform the analysis. Two twins are observed in foil #1, one parallel to the fracture surface (surface twin), the other at an angle to the fracture surface (sub-surface twin), which presumably intersects the surface twin outside the region of the foil. In foil #2, only one corner of the fracture surface interface has been removed (lower left), leaving ample material for

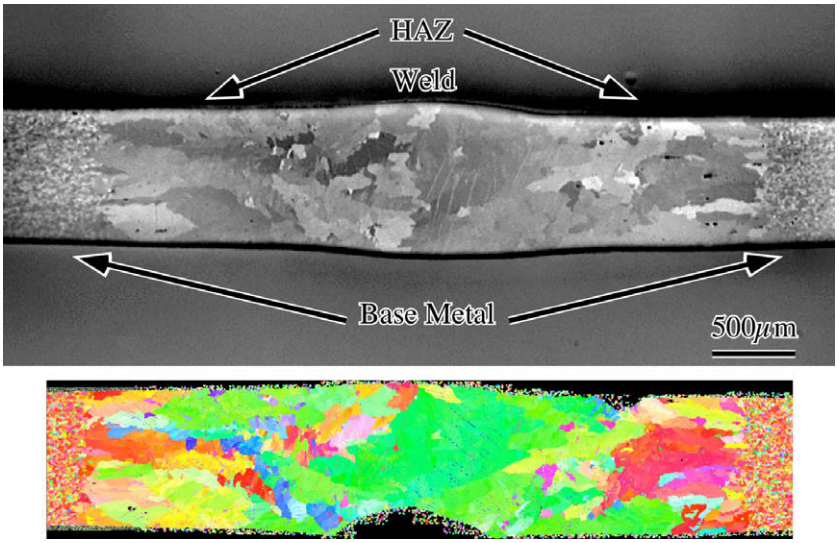

Fig. 1. Optical micrograph (top) and OIM map (bottom) of as-welded specimen. Note the enlarged grains in the weld and heat-affected zone (HAZ). Missing OIM data at bottom center (semi-circular region) is due to carbon paint covering specimen in this area.

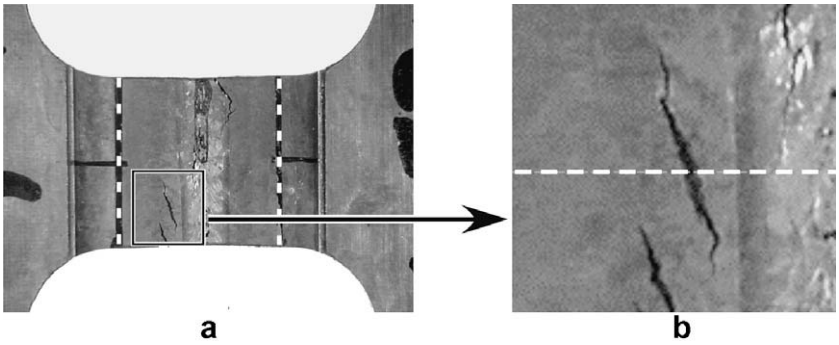

Fig. 2. (a) Tensile bar containing weld after testing. (b) Higher magnification of crack showing cross-section plane.

the line direction analysis (line direction in this analysis refers to a direction contained within the fracture surface plane of the specimen). As in foil #1, two twins are observed, the first is again adjacent to the fracture surface (surface twin) and the second is at an angle to this surface (sub-surface twin). In this case, an intersection between the twins is observed, in which one of the twins crosses the other. Analysis of the twins in both foils is discussed below.

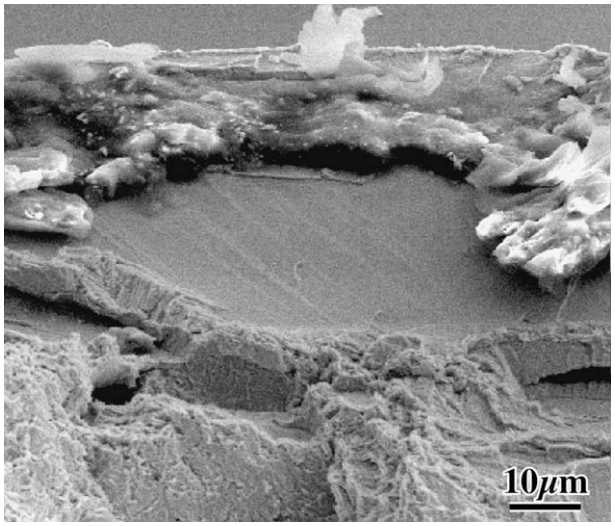

Fig. 3. SEM micrograph showing 'cleavage' facet.

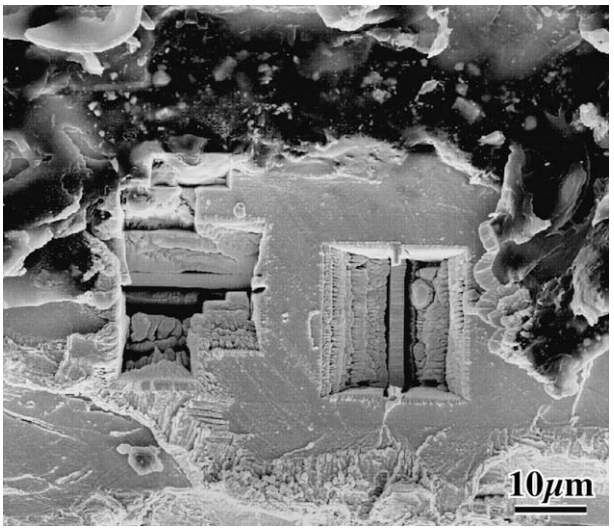

Fig. 4. SEM micrograph showing fracture surface after removal of both foils (#1 on left, #2 on right).

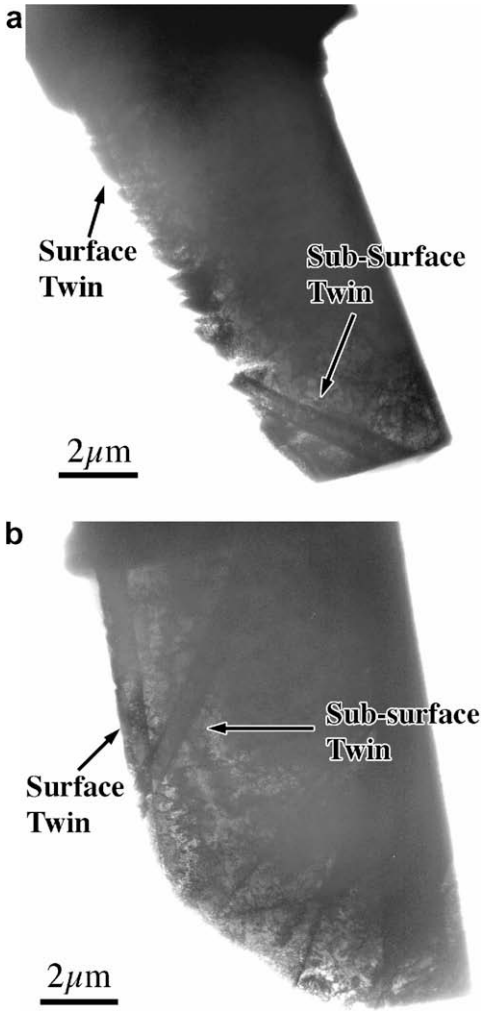

Fig. 5. Low magnification TEM images of FIB foils used in fracture surface determination and analysis of twin interactions. (a) Foil #1 and (b) foil#2.

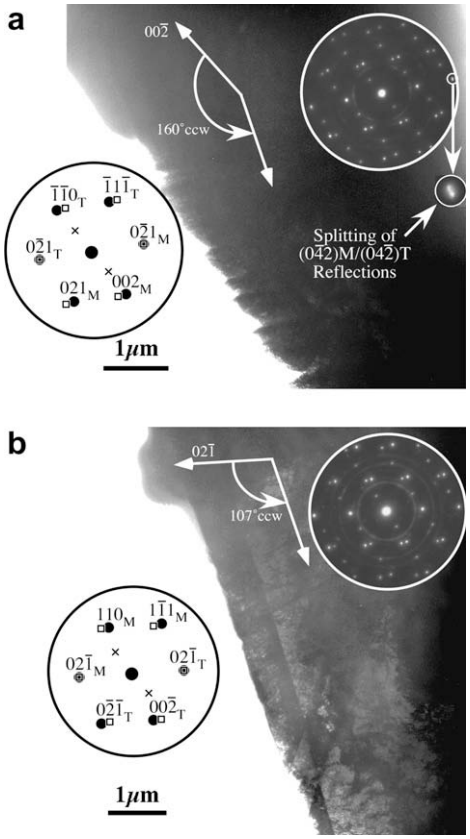

Fig. 6. Example of bright field micrographs and corresponding select area diffraction patterns used to determine fracture plane. (a) Foil #1, (b) foil #2. See text for details.

Examples of micrographs and SAD patterns used to perform a line direction analysis on the edge of each foil are shown in Fig. 6. These edges constitute the intersection of the foil with the fracture surface. Projected line directions were determined by measuring the angle between the foil edge and a known crystallographic plane normal at a specific zone axis. The measurement of these angles is shown in Fig. 6. The actual direction is contained within a plane defined by the projected direction and the zone axis. This plane was traced on a stereographic projection. Plane traces were obtained from two or more zone axes, and the line direction determined as their intersection [16]. Knowledge of the geometry associated with the removal of the foils from the fracture surface (i.e., the 90° angle between them) allowed the establishment of a common set of basis vectors for the foils. The cross-product of the two line directions then yields the fracture plane. All of this was accomplished using the stereographic projection feature of the 'Desktop Microscopist' (Lacuna Laboratories) software package.

Results from the two line direction analyses and the cross-product to determine the fracture plane are presented in Fig. 7. The determined fracture plane is very close (well within the experimental errors associated with the technique) to the $(1\bar{7}2)$ plane. This is the approximate K_1 plane for the surface twin, which was determined using the diffraction data shown in Fig. 6, along with data from other zone axes. Note that two diffraction patterns are superimposed in the SAD patterns, one from the matrix and one from the twin. These were indexed in the common set of basis vectors from the two foils as follows:

Foil 1 : $[100]M||[\bar{1}12]T$
$(0\bar{2}1)M||(02\bar{1})T$
Foil 2 : $[\bar{1}12]M||[100]T$
$(0\bar{2}1)M||(02\bar{1})T$

where 'M' and 'T' represent indices for the matrix and twin, respectively. The first line identifies the zone axes of the patterns in Fig. 6, while the second line represents the aligned {021} planes for the $(1\bar{7}2)$ twin orientation relationship. A slight rotation of the patterns (between the matrix and the twin) is observed for foil #1, such that the two {021} **g**-vectors are slightly misaligned (by ~1°). This is shown in the inset in Fig. 6(a), in which splitting is discernible between the $(0\bar{4}2)$M and $(04\bar{2})$T reflections. This is believed to have been caused by post-twinning deformation near the fracture surface. Since this is a Type II twin, the actual K_1 plane is irrational, but is only ~1° from $(1\bar{7}2)$. This analysis is consistent with previous work in which it was determined that the material fractures (or 'parts') along {172} twin planes.

EBSD was also performed in the vicinity of cracks both in the plan view and for a cross-section mounted specimen. Fig. 8(a) is a plan view inverse pole figure (IPF) map of the large crack near the top of the tensile specimen in Fig. 2 along with a color key of a standard stereographic quadrant for the orthorhombic α-U structure. Fig. 8(b) and (c) are plan view IPF maps of the same grain on either side of the long straight crack shown in the inset in Fig. 2, and Fig. 8(d) is the cross-section view of the same crack although not the same grain. For each image most of the twins are {172}

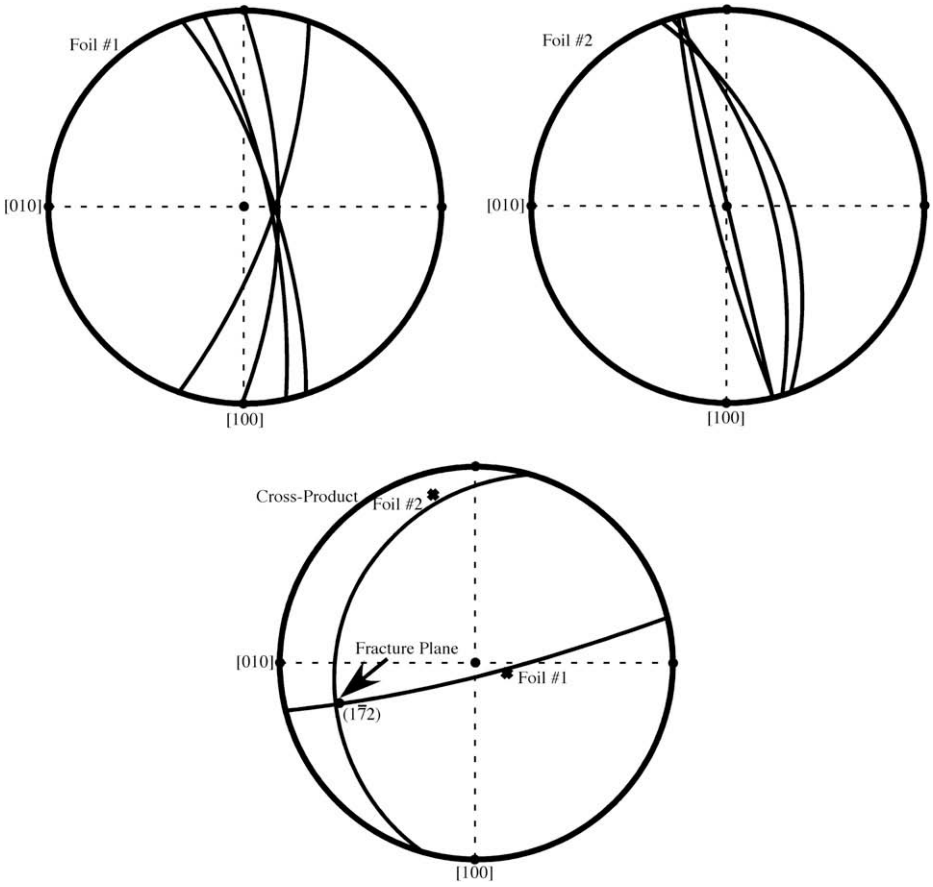

Fig. 7. Schematics of stereographic projections used to determine fracture plane. Top: determination of line directions from individual foils, bottom: determination of fracture plane from line directions.

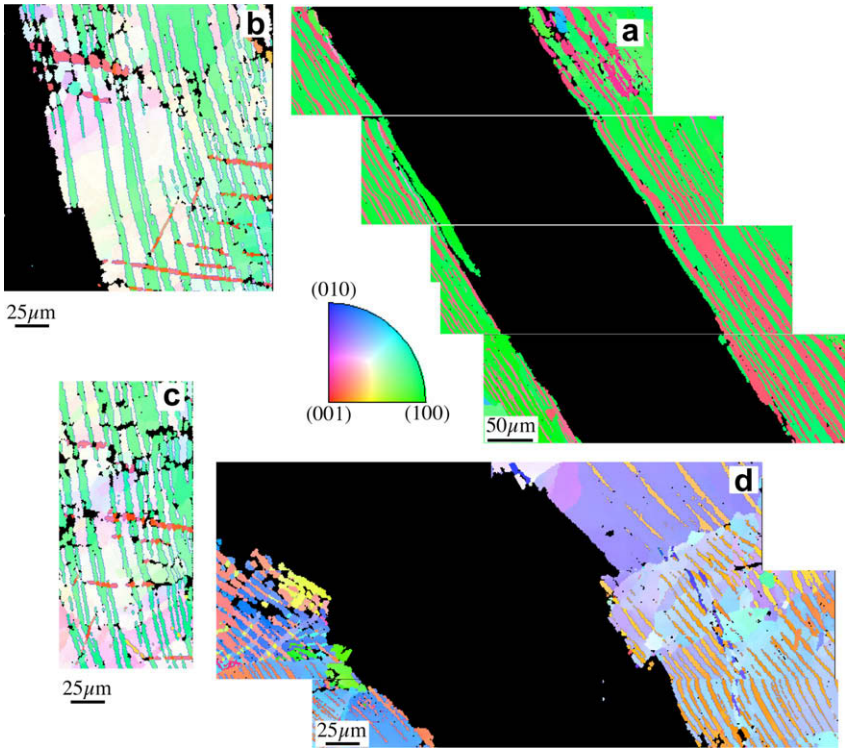

Fig. 8. Low magnification OIM images near fracture surface and orientation key.

type and all of the twins running parallel to the crack are {1 7 2} type. The EBSD data are consistent with the TEM conclusion that the fracture is preferentially occurring parallel to {1 7 2} twins in that {1 7 2} plane traces (and the {1 7 2} twins themselves) run roughly parallel to the cracks. Numerous twin crossings can be observed in Fig. 8(b)–(d) and some of these were investigated in more detail, as discussed below.

3.4. Twin Interactions

Interactions between twins, particularly twin crossings, are of particular interest in α-U. One of the unique aspects found in this material is the ease with which {1 7 2} Type II twins can cross other twins in the structure, including other {1 7 2} twins. Several examples were observed in both the TEM and EBSD investigations of these specimens.

Fig. 9 is a schematic of a twin crossing. According to Cahn [1], one twin can cross another if two conditions are met:

(1) The traces of the crossing (A) and secondary (C) twins in the plane of the crossed twin (B) must be parallel.
(2) The direction (η_1) and magnitude (s) of shear must be identical in the crossing and secondary twins, and the sense of shear must be the same.

For a Type I or compound crossed twin these conditions are always satisfied if the η_1 for the crossing twin (twin A) is contained within the K_1 of the crossed twin (twin B). This can be understood in terms of the transformation that takes place across this type of twin, i.e., a 180° rotation about K_1 of twin B. If the η_1 of the crossing twin (A) is contained within the K_1 of the crossed twin (B), it is rotated to be antiparallel to its original orientation within the matrix, and will still lie within the K_1 plane of B. The K_1 plane of A will also be rotated 180° about the K_1 of B, as will its trace with this plane. The η_1 of A is contained within K_1 of A and K_1 of B, and therefore is parallel to the intersection of these two planes. This intersection is parallel to the intersection of K_1 for the same twinning system within B, giving rise to twin C (within B) with a parallel trace and the same magnitude of shear (since it is the same twinning system). Since both components of A (K_1 and η_1) are antiparallel in B compared to the matrix, the two twinning systems will also have the same sense of shear. The orientation of the K_1 plane of C will be different from that of A (unless the normal of K_1 of A is also contained within the K_1 of B) resulting in a deflection of A as it crosses B. This allows one to determine by inspection which twin is crossing which, even without specific crystallographic information for the twins. The K_1 of the crossed twin (B) is not deflected, since the shear direction of the crossing twin is contained within it. Examples of Type I crossed twins have been observed in U [1] and the α″ martensite (a slight monoclinic distortion of α-U) in a U-13 at.% Nb alloy, which displays shape memory behavior and therefore exhibits many twin interactions [17].

When the crossed twin is Type II, the situation is more complicated since the K_1 plane is irrational and the 180° rotation is about η_1, not K_1, for this type of twin. Cahn analyzed this situation for the case of crossing {1 7 2} twins in α-U [1] and found that all of the twin components of A align to within fractions of a degree with those of the reciprocal {1 1 2} twin in B for certain combinations. Cahn discussed one example of such a crossing. In the present work, all combinations of {1 7 2} twins were considered. The results are given in Table 2.

The fact that all of the twinning components, i.e., K_1, K_2, η_1, and η_2, in the crossing twin (A) are aligned with the components of its reciprocal twin within the crossed twin (B) has several ramifications. First, condition (1) above is automatically met. Second, since a twin and its reciprocal both have the same magnitude of shear, at least one half of condition (2) is met. The other half, that both twins have the same sense of shear, will be discussed below. Third, if twin A can cross twin B, then the reverse is also allowed, as reflected in Table 2. Fourth, there is no deflection of the K_1 plane in moving from the matrix to the crossed twin. These last two points mean that it is not possible to determine which twin is crossing which, even if both twins A and B have been fully indexed.

Sub-surface twins were observed in both FIB/TEM foils and their intersections will now be considered. Diffraction data taken from the sub-surface twin in foil #1 identified it as a $(\bar{1}\,7\,2)$ twin. An example is shown in Fig. 10. Note that this pattern is similar to those shown for the surface twin in Fig. 6, but with the ⟨1 1 2⟩ zone axis from the twin in a mirrored orientation (the pattern in Fig. 7 must be rotated ~45° counterclockwise to make this comparison). According to Table 2, this twin cannot cross the $(1\,\bar{7}\,2)$ surface twin, at least not without accommodation of residual strains by other mechanisms (i.e., a 'forced' crossing). Unfortunately, this intersection was outside the foil region and therefore could not be analyzed.

Table 2
Crossing twins allowed (Y) or forbidden (N).

	$1\,7\,2$	$\bar{1}\,7\,2$	$\bar{1}\,\bar{7}\,2$	$1\,\bar{7}\,2$
$1\,7\,2$		N	N	Y
$\bar{1}\,7\,2$	N		Y	N
$\bar{1}\,\bar{7}\,2$	N	Y		N
$1\,\bar{7}\,2$	Y	N	N	

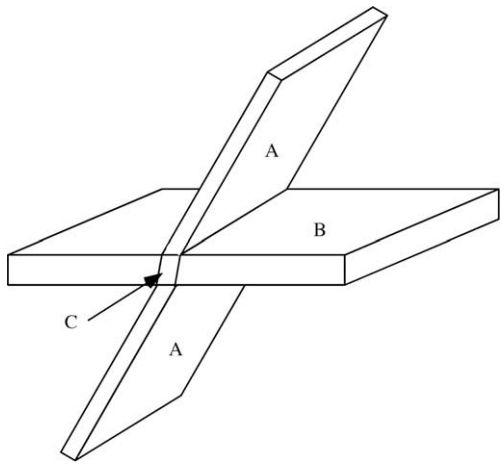

Fig. 9. Schematic showing twin crossings as described by Cahn [1] and discussed in the text.

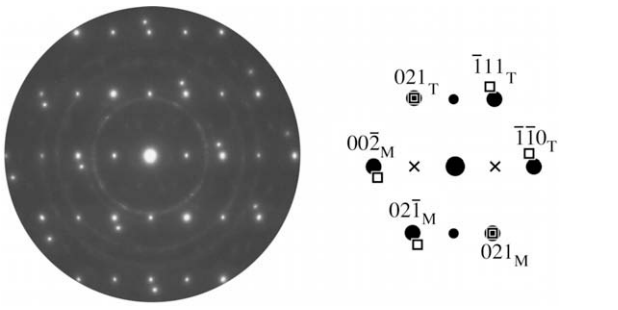

Fig. 10. SAD pattern from the sub-surface twin in foil #1 and indexed schematic. Circles are matrix reflections, squares twin reflections, and x's double diffracted. The twin is indexed as $(\bar{1}\,7\,2)$ and the zones axes are [1 0 0]M and $[\bar{1}\,1\,2]$T.

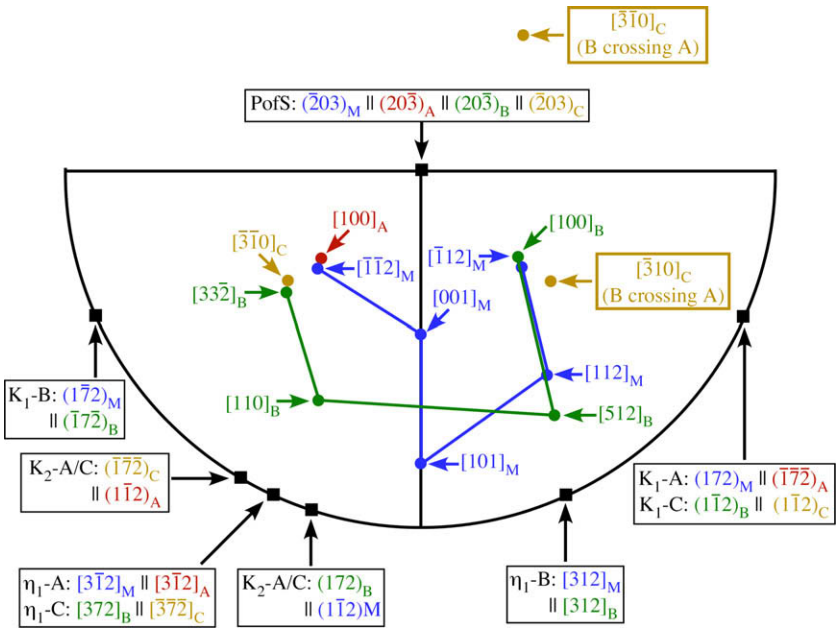

Fig. 11. Stereographic projection showing twinning elements for crossing twins and zone axes used for analysis of twins in foil #2.

In foil #2, this intersection was contained within the foil, allowing a complete analysis. The results are summarized in the stereographic projection of Fig. 11. Because of the orientation of the twin with respect to the foil, only a single zone axis was obtained containing patterns from the matrix and the sub-surface twin. This pattern was similar to the one shown in Fig. 10. With no additional diffraction data, a unique identification could not be made. Thus the twin could only be identified as either $(\bar{1}72)$ or (172). However, since there appears to be a crossing between the surface and sub-surface twins, the latter was tentatively identified as (172), according to the rules listed in Table 2. This identification was confirmed by additional analysis, as described below.

As discussed above, even with both twins identified, the question of which crosses which (i.e., which twin came first) cannot be answered. However, this question can be resolved by analyzing twin C, as shown in Fig. 11. In the Figure, all of the zone axes collected during the analysis are shown as colored circles, with the colors designating the matrix and three different twins, as shown in Table 3. The plane of shear for all of the twins has been placed in the center of the projection so that the relevant elements appear on the circumference, designated with black squares and indexed with the same color coding used for the zone axes. Note that the sub-surface twin is identified as A, the crossing twin. The justification for this choice will be given below.

Two important points can be gleaned from Fig. 11:

(1) All of the twinning elements are aligned and the sense of shear is the same for A and C, as determined by Cahn [1] in his original analysis. The latter point can be demonstrated by considering the positions of the K_2 planes for twins A and C. The K_2 plane for twin A, indexed with respect to the matrix (M), and twin C, indexed with respect to twin B, are aligned on one side of the η_1 direction. These represent the position of K_2 before the twinning shear. These same planes indexed with respect to twin A and twin C, respectively, indicating the position after shear, are on the opposite side of η_1.

(2) The position of the $[\bar{3}\,\bar{1}\,0]$ zone axis, taken from twin C, is indicated on the figure. This zone axis was found experimentally to be nearly aligned with the $[3\,3\,\bar{2}]$ zone axis of B, consistent with the designation of the sub-surface twin as the crossing twin. The positions of the $\langle 1\,3\,0\rangle$ zone axes of C for the case of the surface twin being the crossing twin (i.e., B crossing A) are also shown, and are clearly inconsistent with the experimental data. Therefore, analysis of twin C can distinguish between the crossing and crossed twin, a distinction that cannot be made without this information. In the case at hand, the sub-surface twin has crossed the surface twin.

Table 3
Indexing scheme for twin crossing in foil #2 and color key for Fig. 11.

Twin	K_1	K_2	η_1	η_2	Color
A	(172)	$(1\bar{1}2)$	$[3\bar{1}2]$	$[372]$	Red
B	$(1\bar{7}2)$	(112)	$[312]$	$[3\bar{7}2]$	Green
C	$(1\bar{1}2)$[a]	(172)[a]	$[372]$[a]	$[3\bar{1}2]$[a]	Orange
Matrix	–	–	–	–	Blue

[a] Indexed with respect to twin B. K_2 and η_1 are reversed within twin C.

In practice, the data need not be analyzed at this level of detail. All that is required is to determine which intersecting twin has a twin relationship with C. This will be the crossed twin. Indeed the position of the $[\bar{3}\,\bar{1}\,0]$ zone axis that is consistent with the experimental data in the stereographic projection of Fig. 11 assumes this twin orientation relationship between B and C, even though this relationship could not be determined directly from the available diffraction data. This determination is particularly straight forward in EBSD.

An analysis of a similar situation was performed using EBSD. Fig. 12 shows an enlarged area from an IPF map in which two $\{172\}$ twins are crossing. They were identified as $(\bar{1}72)$ and $(\bar{1}\bar{7}2)$ twins and are allowed to cross according to Table 2. If the $(\bar{1}72)$ twin is labeled twin A the $(\bar{1}\bar{7}2)$ as twin B, B and C share a $(\bar{1}12)$ twin orientation relationship, the reciprocal of $(\bar{1}\bar{7}2)$, consistent with A crossing B.

One last case will be considered, in which a crossing is observed between a $(\bar{1}72)$ and $(\bar{1}\,\bar{1}\,2)$ twin, as identified using EBSD and shown in Fig. 13. Although $\{1\,7\,2\}$ twins can sometimes cross $\{1\,1\,2\}$ twins, this is not an allowed crossing in this case, since

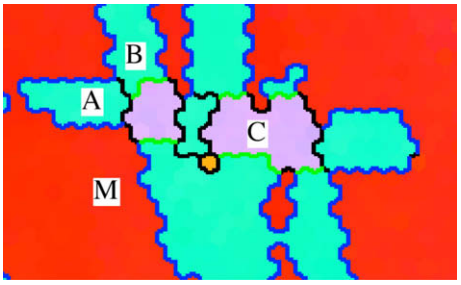

Fig. 12. OIM analysis of crossing {1 7 2} twins. See text for details.

the $[\bar{3}\,1\,2]$ η_1 direction for the $(\bar{1}\,\bar{7}\,2)$ twin is not contained within the $(\bar{1}\,\bar{1}\,2)$ K_1 plane. It then must be considered under what circumstances a {1 1 2} twin can cross a {1 7 2} twin, a phenomenon that has not been previously observed, but was predicted by Cahn [1]. It should be noted that $(\bar{1}\,\bar{1}\,2)$ is the reciprocal of $(\bar{1}\,7\,2)$, which can cross a $(\bar{1}\,\bar{7}\,2)$ twin, as noted above. A $(\bar{1}\,\bar{1}\,2)$ twin crossing a $(\bar{1}\,\bar{7}\,2)$ can take place because all of the twinning elements of the two twins are aligned. Since the reciprocal twin is derived by exchanging these twinning elements (i.e., $K_1 \leftrightarrow K_2$ and $\eta_1 \leftrightarrow \eta_2$), the reciprocal twin should also be able to cross. Note that there is no deflection of the crossing twin in this case either. However, since the $(\bar{1}\,\bar{7}\,2)$ twin cannot cross the $(\bar{1}\,\bar{1}\,2)$ twin, analysis of the intersection is not necessary to identify the crossing twin. Nevertheless, a $(\bar{1}\,7\,2)$ twin orientation relationship was identified between B and C, confirming the analysis. The allowed {1 1 2}/{1 7 2} crossings are summarized in Tables 4 and 5. Table 4 is generated by considering the reciprocals of the {1 7 2} twins in the top row of Table 2. The diagonal of the table considers whether a {1 1 2} twin can cross its reciprocal. This crossing is not allowed. Table 5 is generated by determining whether the η_1 of the {1 7 2} is contained within the K_1 plane of the {1 1 2}, as discussed above.

The detailed analysis of the TEM data shown in Fig. 11 and the EBSD data in Figs. 12 and 13 demonstrate that the ambiguity between the crossed and crossing twin can be resolved by considering the crystallographic orientation relationship between the intersection twin (twin C) and the two intersecting twins.

Finally, some discussion of the role of twinning in plasticity and fracture in this material is warranted. As in other materials, twinning in α-U has a positive effect on plasticity by contributing to deformation when an insufficient number of slip systems is available. {1 7 2} and {1 1 2} twinning are two of the few uranium deformation mechanisms that will accommodate strain in tension near the [0 0 1] direction [5], and these twins are numerous in the HAZ of our welded samples, particularly in grains oriented near [0 0 1]. However, for reasons unknown, the {1 7 2} twin interfaces also provide favorable sites for either crack initiation or propagation, resulting in 'parting' fracture along these boundaries as discussed above. The {1 7 2} twins extend over large distances because of the very large grains present in the HAZ, so that fracture can easily propagate over large distances as well. Thus, twinning permits additional plasticity, but also contributes to premature failure in the very large grains present in the HAZ region. The rapid decrease in ductility of α-U above a critical grain size has in fact been attributed to the grain size exceeding the critical crack length for fracture by previous investigators [9].

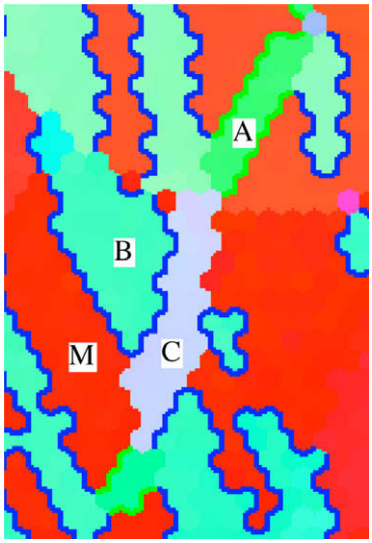

Fig. 13. OIM analysis of {1 1 2} twin crossing {1 7 2} twin. See text for details.

Table 4
{1 1 2} crossing {1 7 2}: allowed (Y) or forbidden (N).

	$1\,\bar{1}\,2$	$\bar{1}\,\bar{1}\,2$	$\bar{1}\,1\,2$	$1\,1\,2$
$1\,7\,2$	N	N	N	Y
$\bar{1}\,7\,2$	N	N	Y	N
$\bar{1}\,\bar{7}\,2$	N	Y	N	N
$1\,\bar{7}\,2$	Y	N	N	N

Table 5
{1 7 2} crossing {1 1 2}: allowed (Y) or forbidden (N).

	$1\,7\,2$	$\bar{1}\,7\,2$	$\bar{1}\,\bar{7}\,2$	$1\,\bar{7}\,2$
$1\,\bar{1}\,2$	N	N	Y	N
$\bar{1}\,\bar{1}\,2$	N	N	N	Y
$\bar{1}\,1\,2$	Y	N	N	N
$1\,1\,2$	N	Y	N	N

4. Conclusions

The application of modern analytical techniques to the problems of deformation twinning and fracture can result in a more detailed characterization and understanding of these phenomena. Specifically, in the case of α-U, the following observations have been made:

- The fracture surface has been confirmed as {1 7 2}, associated with 'parting' along {1 7 2} twins.
- The ambiguity of crossing vs. crossed twins for the case of {1 7 2} has been resolved by crystallographic analysis of the intersection (twin C).
- The first observation of a {1 1 2} twin crossing a {1 7 2} twin has been made.

Acknowledgments

The authors wish to thank Dr Paul Burgardt and Andrew Duffield for welding the specimens and Michael Mauro for performing the mechanical tests. Ann Kelly is also gratefully acknowledged for optical metallography and Pallas Papin for preparing the FIB foils. This work was performed under contract number DE-AC52-06NA25396 with the US Department of Energy.

The authors also wish to take this opportunity to note the recent passing of Professor Robert W. Cahn, whose seminal paper, published in the first issue of Acta Metallurgica, laid much of the groundwork for the understanding of deformation in α-U and other low symmetry structures, not the least of his many contributions to the field of materials science.

References

[1] R.W. Cahn, Acta Metall. 1 (1953) 49.
[2] A.G. Crocker, J. Nucl. Mater. 16 (1965) 306.
[3] F.C. Frank, Acta Metall. 1 (1953) 71.
[4] L.T. Lloyd, H.H. Chiswik, Trans. AIME 203 (1955) 1206.
[5] J.S. Daniel, B. Lesage, P. Lacombe, Acta Metall. 19 (1971) 163.
[6] A. Lemongne, P.J. Lacombe, Nucl. Mater. 8 (1963) 116.
[7] A. Lemongne, P.J. Lacombe, Nucl. Mater. 16 (1965) 129.
[8] D.M.R. Taplin, J Aust. I. Met. 12 (1967) 32.
[9] G.T. Newman, C.J. Beevers, J. Nucl. Mater. 23 (1967) 95.
[10] J.F. Bingert, R.J. Hanrahan Jr., R.D. Field, P.O. Dickerson, J. Alloys Compd. 365 (2004) 138.
[11] R.J. McCabe, D.F. Teter, J. Microsc. 223 (2006) 33.
[12] G.T. Gray III, C.M. Cady, R.J. McCabe, R.S. Hixson, D.R. Korzekwa, M.F. Lopez, J. de Phys., IV 134 (2006) 909.
[13] D.W. Brown, M.A.M. Bourke, B. Clausen, D. Korzekwa, R. Korzekwa, R.J. McCabe, T.A. Sisneros, D.F. Teter, Mater. Sci. Eng. A, in press.
[14] R.E. Hackenberg, R.D. Field, P.A. Papin, J.C. Cooley, D.F. Teter, Ultramicroscopy 107 (2007) 698.
[15] A.M. Kelly, D.J. Thoma, R.D. Field, P.S. Dunn, D.F. Teter, J. Nucl. Mater. 353 (2006) 158.
[16] M.H. Loretto, R.E. Smallman, Defect Analysis in Electron Microscopy, Chapman and Hall, London, 1975.
[17] R.D. Field, D.J. Thoma, P.S. Dunn, D.W. Brown, C.M. Cady, Philos. Mag. A 81 (2001) 1691.